Lekbir *et al. Energy Mater.* **2025**, *5*, 500101
**DOI:** 10.20517/energymater.2025.46

**Energy Materials**

**Article**

**Open Access**

# Performance and environmental impact analysis of thermoelectric generators through material selection and geometry optimization

**Abdelhak Lekbir[1,3], Saad Mekhilef[2,3,*], Kok Soon Tey[1], Abdullah Albaker[4]**

[1]Department of Computer System & Technology, Faculty of Computer Science and Information Technology, Universiti Malaya, Kuala Lumpur 50603, Malaysia.
[2]School of Engineering, Swinburne University of Technology, Hawthorn, VIC 3122, Australia.
[3]Power Electronics and Renewable Energy Research Laboratory (PEARL), Department of Electrical Engineering, Universiti Malaya, Kuala Lumpur 50603, Malaysia.
[4]Department of Electrical Engineering, College of Engineering, University of Ha'il, Ha'il 10 City 81451, Saudi Arabia.

***Correspondence to:** Prof. Saad Mekhilef, School of Engineering, Swinburne University of Technology, John Street, Melbourne, VIC 3122, Australia. E-mail: smekhilef@swin.edu.au

**How to cite this article:** Lekbir, A.; Mekhilef, S.; Tey, K. S.; Albaker, A. Performance and environmental impact analysis of thermoelectric generators through material selection and geometry optimization. *Energy Mater.* **2025**, *5*, 500101. https://dx.doi.org/10.20517/energymater.2025.46

**Received:** 26 Feb 2025 **First Decision:** 8 Apr 2025 **Revised:** 22 Apr 2025 **Accepted:** 25 Apr 2025 **Published:** 14 May 2025

**Academic Editors:** Sung Son Jae, Sen Xin **Copy Editor:** Fangling Lan **Production Editor:** Fangling Lan

## Abstract

This study evaluates the performance and environmental impact of thermoelectric generators (TEGs) by analyzing various thermoelectric materials and system geometries. A comprehensive life cycle assessment is conducted to quantify the embodied energy and carbon emissions associated with different materials. The study employs particle swarm optimization to optimize TEG geometry, aiming to enhance power output while minimizing environmental impact. The results demonstrate that material selection significantly influences both energy conversion efficiency and sustainability. Specifically, PbTe-based TEGs achieve the highest power output, whereas SiGe-based modules exhibit the highest environmental footprint. Through optimization, an 80% increase in power output is achieved for certain configurations, alongside a reduction in $CO_2$ emissions. Key findings highlight PbTe-based TEGs as the most efficient energy converters, while $Bi_2Te_3$-based modules strike a balance between performance and sustainability. In contrast, SiGe-based TEGs have the highest environmental footprint due to their high embodied energy. Additionally, the study reveals that optimizing the number of thermocouples and leg dimensions significantly improves energy conversion efficiency and reduces carbon emissions. These findings provide valuable insights for designing next-generation TEG systems that effectively balance performance and environmental responsibility.

**Keywords:** TEG materials, leg geometry, geometry optimization, embodied energy, environmental impact.

## INTRODUCTION

The global energy demand has significantly increased due to the widespread use of electronic devices[1]. In this context, the world faces two major challenges: meeting the growing energy demand and reducing the environmental impact associated with traditional power plants[2]. Renewable energy sources, such as wind, solar, and thermal, can offer sustainable power generation[3]. Various systems have been introduced to harvest these energy sources and convert them into electricity including conventional energy conversion methods, such as wind turbines, or microscale technologies, such as thermoelectric generators (TEGs)[4].

TEGs are solid-state devices that convert temperature gradients between hot and cold sides into electricity[5]. These devices rely on thermoelectric materials that transport charge carriers and phonons, enabling direct heat-to-electricity conversion[6]. TEG modules are compact, scalable, and can be easily integrated into systems where a temperature gradient is present[7]. In several applications, TEG modules have demonstrated unique potential for waste heat harvesting[8]. Numerous studies have explored TEG integration in solar energy systems, automotive applications, and industrial waste heat recovery, resulting in diverse module designs with varying materials and sizes[9]. The findings indicate that these TEGs can operate continuously as long as a temperature difference is maintained, making them a favorable option for power generation in applications where other renewable energy systems experience intermittent production[10]. However, while their efficiency is lower compared to other renewable sources, advancements in materials have improved their performance[11]. In this context different studies have examined the impact of material selection on TEG performance, evaluating both traditional thermoelectric materials (e.g., $Bi_2Te_3$, PbTe, and SiGe) and recently developed alternatives such as $CoSb_3$, GeTe, $Sn_XSe$, BiCuSeO, SWNTs/PEDOT, $Bi_{0.48}Sb_{1.52}Te_3$ + graphene[12], *etc*. Other researchers explore the performance of flexible TEGs using advanced materials, where the flexibility of the materials is crucial for applications in wearable devices, portable electronics, and other flexible energy harvesting systems[13-16]. However, these studies mainly assess TEG efficiency based on key material parameters, overlooking environmental impact and long-term performance, both crucial for commercial scalability.

Recently, several studies have investigated the environmental impact of TEG materials. Chan *et al.* analyzed four commercial TEG modules, assessing efficiency, reliability, and long-term performance[17]. However, their study highlighted gaps in data on material properties, size limitations in commercial models, and the lack of a detailed greenhouse gas (GHG) emissions analysis. Lan *et al.* examined the environmental and economic impact of TEG leg geometry and structure, considering material properties and heat dissipation[18]. Their findings suggest that optimizing TEG configurations can reduce $CO_2$ emissions by 1.0%-72.1%, especially for low hot-source temperatures and high-ZT materials. However, these modifications adversely affect economic viability and thermal efficiency. Ibn-Mohammed *et al.* conducted a comprehensive analysis of the techno-environmental impact of various TEG modules, highlighting the significant influence of material selection[19]. Their findings show that fabrication requires substantial electrical energy, with non-oxide materials such as $Bi_2Te_3$ posing high toxicity risks due to tellurium and antimony. In contrast, oxide-based materials demonstrate lower toxicity but are associated with higher environmental impacts of cobalt oxide. Soleimani *et al.* assessed the environmental impact of TEG materials during production, considering resource consumption, emissions, waste, energy demand, and global warming potential[20]. Their analysis of inorganic, organic, and hybrid materials revealed that inorganic types generally have the highest impact due to energy-intensive manufacturing, except for $Bi_2Te_3$, which had the lowest impact among all studied materials. These studies highlight the growing concern regarding the environmental footprint of TEG materials, yet significant research gaps remain. Therefore, advancing sustainable TEG systems requires further research to optimize energy conversion efficiency while

minimizing environmental impact.

### Contributions of this study

Upon reviewing the existing literature, it is clear that most published works have primarily focused on enhancing the performance of TEG modules by integrating different types of materials. However, only a limited number of studies have examined their environmental impacts despite this being a critical aspect of any renewable technology. Moreover, most studies on the environmental impact of different TEG materials consider TEG modules of similar sizes, typically referring to commercial TEG modules. Additionally, research investigating the environmental impact of TEG materials throughout their production phases, including raw material supply, transportation to the manufacturing site, and final material fabrication, often lacks sufficient data, particularly for the latter two stages. This limitation arises because different TEG raw materials require distinct processing equipment and varying energy inputs for transformation and manufacturing, leading to non-generalizable results and making comparative studies impractical. Furthermore, most existing studies focus either on material selection or geometric optimization, often neglecting a holistic approach that integrates both aspects through innovative multi-objective optimization. Moreover, the trade-offs between environmental benefits and performance efficiency remain insufficiently explored. This study presents a comprehensive approach to TEG module design to address these gaps by integrating performance assessment with environmental impact evaluation. Specifically, the optimization of TEG system geometry is conducted using particle swarm optimization (PSO)-based multi-objective optimization to simultaneously maximize power output and minimize environmental impact. By refining design parameters, this approach enhances efficiency while reducing material-related emissions, paving the way for next-generation TEG modules that are both high-performing and sustainable. Overall, the findings provide valuable insights for researchers, policymakers, and industry professionals seeking to improve the sustainability and efficiency of thermoelectric energy conversion systems.

## METHODS

This study investigates the performance and environmental impact of various TEGs. The analysis is based on the geometry of commercially available TEGs and the different types of TEG materials commonly used in previous research. While the input parameters are derived from experimentally validated data reported in the literature, this study employs a novel computational framework to generate new insights. Specifically, the methodology involves advanced modeling, performance optimization, and environmental impact assessment, which extend beyond the scope of the original experimental studies. By leveraging validated data, this approach enables a comprehensive evaluation of TEG materials and designs without the need for additional experimental validation, ensuring both reliability and the generation of original findings.

In this context, Several assumptions have been considered to achieve the main objectives of the present study. These assumptions are outlined as follows:

1. A temperature difference of 30 K is assumed. This value is a realistic and conservative estimate for low-grade waste heat recovery system applications.

2. The TEG module is assumed to have a 20-year operational lifespan. This is justified by the high durability and absence of moving parts in TEG systems, which align with the typical lifespan of photovoltaic (PV) systems.

3. TEG systems are solid-state devices that require negligible maintenance due to the absence of mechanical components or moving parts. This aligns with standard assumptions for long-term applications of solid-

state technologies.

4. It is assumed that the TEG system experiences no significant performance degradation over its lifespan. Minor degradation from oxidation or thermal cycling is estimated to occur in real-world scenarios, but its impact is minimal for encapsulated modules under stable thermal gradients.

5. The estimated environmental impact is primarily attributed to the embodied energy associated with the raw materials used in the TEG module. Variations in processing techniques and energy inputs across different stages of the TEG lifespan lead to non-generalizable outcomes, complicating direct comparisons and limiting the practicality of broader studies.

### System geometry

A TEG module is a solid-state device that converts heat into electricity through the Seebeck effect. It consists of multiple thermoelectric couples, typically made from semiconductor materials, arranged in a series of p-type and n-type legs connected by a conductive electrode. These legs are sandwiched between two ceramic plates, which provide mechanical support, facilitate heat transfer, and ensure electrical insulation. When a temperature difference is applied, charge carriers move from the hot to the cold side, generating electricity. The schematic 3D geometry of TEG module is presented in Figure 1. TEG efficiency is fundamentally influenced by material properties, the temperature gradient, and the system design. For instance, the design factors play a pivotal role in determining the overall performance of the module. Specifically, the arrangement of thermocouples directly influences internal resistance and voltage output, while the selection of electrode materials governs electrical conductivity and thermal stability. Additionally, the ceramic plates are crucial for ensuring effective thermal insulation and heat transfer. Consequently, optimizing the geometry of the TEG module, with careful consideration of these factors, is essential for maximizing its thermoelectric performance and overall operational efficiency.

Commercial TEG modules are available in various system geometries, sizes, material compositions, and power ratings. This study considers different types of TEG materials to evaluate the performance of TEG modules with a standardized geometry. The dimensions of the various components in these TEG modules are equivalent to those of the most common commercial TEG module. The detailed dimensions of commercial TEG components are presented in Table 1.

### Performances calculation

The output of a TEG module depends on several factors, including the temperature gradient (ΔT), the Seebeck coefficient ($S$), internal resistance ($R_{s,TEG}$), and the number of thermocouples ($n$). This study uses different materials for various types of TEGs. Since different materials have varying Seebeck coefficients and electrical resistivities, material selection plays a crucial role in performance. Ideally, materials used in TEG applications should exhibit a high Seebeck coefficient, high electrical conductivity, and low thermal conductivity to maximize electrical performance. The equivalent Seebeck coefficient for each TEG module is summarized in Table 2.

Once the equivalent Seebeck coefficient (S) for each TEG module is determined, the open-circuit voltage can be evaluated using[42]:

$$V_{oc} = n \times S \times \Delta T \quad (1)$$

**Table 1. Dimension of the different components for commercial TEG module**

| Item | Leg dimension (mm) | Number of p and n legs | Copper electrode (mm) | Number of electrodes | Ceramic cover (mm) |
|---|---|---|---|---|---|
| Size | 2 × 2 × 3.4 | 256 | 2 × 2 × 0.3 | 128 | 40 × 40 × 0.5 |

**Table 2. The seebeck and the internal resistances for each leg of TEG**

| Ref | Material structure | TEG leg | *S* for legs (μV/K) | $\rho$ (m Ω/cm) | *S* (μV/K) | $R_{s,TEG}$ (Ω) |
|---|---|---|---|---|---|---|
| TEG1 | $Si_{0.97}Ge_{0.03}$ (P, As) | n-type | -173[21] | 25[22] | 173 | 3.32 |
| | $Si_{0.97}Ge_{0.03}$ (B) | p-type | +173[21] | 25[22] | | |
| TEG2 | $Bi_2Se_{0.3}Te_{2.7}$ | n-type | -170[23] | 1.3[24] | 176.4 | 0.173 |
| | $Bi_{0.5}Sb_{1.5}Te_3$ | p-type | +182.8[25] | 1.3[24] | | |
| TEG3 | $Mg_{3.2}Bi_{1.498}Sb_{0.5}Te_{0.002}$ | n-type | -210[26] | 11[27] | 207 | 0.817 |
| | $Bi_{0.4}Sb_{1.6}Te_3$ | p-type | +204[28] | 1.3[24] | | |
| TEG4 | PbTe | n-type | -343.1[29] | 1.49[30] | 294.73 | 0.198 |
| | PbSnTe | p-type | + 246.3[29] | 1.49[30] | | |
| TEG5 | $Bi_2Te_3$ | n-type | –160[31] | 6.32[32] | 220 | 0.709 |
| | $Sb_2Te_3$ | p-type | +280[33] | 4.36[34] | | |
| TEG6 | $Bi_2Te_3$ | n-type | –160[31] | 6.32[32] | 160 | 0.839 |
| | $Bi_2Te_3$ | p-type | +160[31] | 6.32[32] | | |
| TEG7 | $CoSb_3$ | n-type | -220[35] | 25[36] | 210 | 3.52 |
| | $Zn_4Sb_3$ | p-type | +200[37] | 28[38] | | |
| TEG8 | SiGe | n-type | -200[39] | 1.2[40] | 217.5 | 0.442 |
| | $Tl_9BiTe_6$ | p-type | +235[41] | 5.5[41] | | |

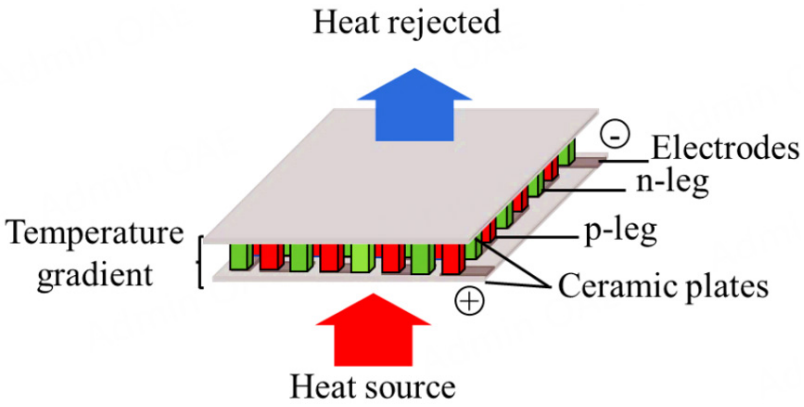


**Figure 1.** The schematic 3D geometry of the commercial TEG module.

On the other hand, the short-circuit current for the TEG module can be calculated using[42]:

$$I_{sc} = \frac{V_{oc} - V_{TEG}}{R_{s,TEG}} \quad (2)$$

where $V_{TEG}$ represents the TEG output voltage which varied between 0 and $V_{oc}$; $R_{s,TEG}$ is the internal TEG module resistance and can be calculated as follows[43]:

$$R_{s,TEG} = \rho \frac{L}{A} \tag{3}$$

where $L$ is the length of the TEG legs, $A$ is the cross-sectional area of the TEG leg, and $\rho$ denotes the electrical resistivity of the TEG material, as summarized in Table 2.

After evaluating the current and voltage outputs, the power output of the TEG can be determined using[42]:

$$P_{TEG} = \frac{(I_{TEG} \times V_{oc}) - (V_{TEG})^2}{R_{s,TEG}} \tag{4}$$

### System inventory input

Before assessing the environmental impact of the materials used in the manufacturing process of a TEG module, it is essential to analyze its energy inventory first. Fundamentally, a TEG module consists of multiple thermocouples connected in series. Each thermocouple comprises two legs, designated as n-type and p-type, which are composed of a mixture of different semiconductor materials. To determine the embodied energy associated with each mixture, several methodological steps must be undertaken. This subsection summarizes the key formulas and methods used to conduct this analysis. The total embodied energy ($CEC$) for each mixture material is dependent on the embodied energy index $EI_i$ for each element $i$. The values for ($EI_i$) are obtained from the literature; therefore, the $CEC$ can be calculated as follows[44]:

$$CEC = \sum(\omega_i \times m_{total} \times EI_i) \tag{5}$$

where $\omega_i$ represents the mass fraction of element $i$ (%), and it can be calculated as follows[45]:

$$\omega_i = \frac{n_i \times M_i}{\sum(n_i \times M_i)} \tag{6}$$

where $n_i$ and $M_i$ are the molar ratio and mass of element $i$, respectively.

The total mass ($m_{total}$) for TEG leg represents the sum for all mass of each element $i$, (g) and it can be calculated as follows:

$$m_{total} = \rho_{composite} \times V \tag{7}$$

where $V$ represents the volume of TEG leg ($cm^3$), and $\rho_{composite}$ represents composite density ($g/cm^3$), and it can be calculated as follows[46]:

$$\rho_{composite} = \frac{1}{\sum\left(\frac{\omega_i}{\rho_i}\right)} \tag{8}$$

where $\rho_i$ is the density of pure element $i$ ($g/cm^3$).

### Environmental impact

The environmental impact of the TEG is dependent mainly on the energy used during the manufacturing phase. Therefore, the amount of emission related to the manufacturing phase ($EP_p$) for the different TEG materials can be determined as follows[2]:

$$EP_p = CExC \times F_p \tag{9}$$

where $CExC$ represents the total exergy consumption equivalent to 36% of the CEC[47]. $F_p$ is the emission factor for the element $\rho$ corresponding to the emission factors for electricity production from coal power plants (i.e., $CO_2$ = 8.68 × $10^{-1}$ kg/m² and GWP = 9.12 × $10^{-1}$ kg.$CO_2$.eq)[48].

### Optimization of the TEG geometry using the PSO method

In the present study, the PSO algorithm is applied to optimize the geometry of TEG legs. PSO is a metaheuristic optimization technique inspired by the collective behavior of birds flocking and fish schooling. It is widely used in engineering, artificial intelligence, and other fields to solve complex optimization problems by iteratively improving candidate solutions based on a population-based search approach[49]. In this study, the optimization of TEG geometry using PSO focuses on three main geometric parameters: the number of legs ($n$), leg length ($l_{leg}$), and leg cross-sectional area ($A_{leg}$). The optimization of these parameters directly enhances the performance of the TEG, improving heat transfer, electrical output, and overall efficiency, while minimizing material usage and ensuring practical feasibility.

The optimization process begins by initializing candidate solutions that include the values for $n$, $l_{leg}$ and $A_{leg}$. The search space is constrained within the boundaries $1 < l_{leg} < 4$ mm and $1 < A_{leg} < 3$ mm². The value of $n$ is determined based on the geometric constraints of $l_{leg}$ and $A_{leg}$ to ensure feasibility in practical applications. For this study, the PSO parameters are set with a swarm size of 50 particles and a maximum of 100 iterations, which balances computational efficiency and solution accuracy. The framework of the PSO-based optimization approach for TEG leg geometry is summarized in Figure 2.

The movement of each particle in the search space is governed by two fundamental update equations: velocity update and position update. The updating equations for the velocity ($V_i$) and position ($X_i$) of the $i$-th generation ($i$ = 1, 2, 3 …., $N$) particles are defined as follows[50]:

$$V_{i+1} = \omega V_i + c_1 r_1 (P_{best,i} - X_i) + c_2 r_2 (G_{best,i} - X_i) \tag{10}$$

$$X_{i+1} = X_i + V_{i+1} \tag{11}$$

where $\omega$, $c_1$ and $c_2$, $r_1$ and $r_2$ are inertia weight ($\omega$ = 0.7), acceleration coefficients ($c_1 = c_2 = 2$), and the random number between 0 and 1, respectively. $P_{best,i}$ and $G_{best,i}$ are the best and the global position of the particle, respectively.

## RESULT AND DISCUSSION

This analysis mainly focuses on the impact of the different types of materials and system geometry on the performance of the TEG. This section presents the obtained results of the present study. The obtained results are based on the type of materials and system geometry. In addition, the result of the different geometry for commercial TEG modules and optimized geometry is also presented and discussed.

### Energy inventory for different TEG materials

The energy inventory of different TEG modules considered in the present study depends on the materials type contained in the present study. This section presents a comprehensive analysis of the different TEG modules to determine the total energy consumed over the manufacturing phase of the different TEG modules. The obtained results are summarized in Table 3.

**Table 3. Equivalent CEC for each TEG module**

| Ref | Leg | Equivalent $EI_i$ for leg materials (MJ/kg) | Material density ($g/cm^3$) | Leg weight (g) | CEC for leg (MJ/leg) | CEC for TEG module (MJ) |
|---|---|---|---|---|---|---|
| TEG1 | n-type | 151.82 | 2.43 | 0.0330 | 5.02 | 1284.38 |
| | p-type | 151.82 | 2.43 | 0.0330 | 5.02 | |
| TEG2 | n-type | 141.2 | 7.64 | 0.1039 | 14.67 | 3567.34 |
| | p-type | 143.76 | 6.75 | 0.0918 | 13.2 | |
| TEG3 | n-type | 144.6 | 5.26 | 0.0715 | 10.34 | 2991.05 |
| | p-type | 143.77 | 6.66 | 0.0906 | 13.02 | |
| TEG4 | n-type | 150 | 8.64 | 0.1175 | 17.63 | 4186.6 |
| | p-type | 136.9 | 8.10 | 0.1102 | 15.08 | |
| TEG5 | n-type | 143.74 | 7.7 | 0.1047 | 15.05 | 3531.28 |
| | p-type | 143.78 | 6.41 | 0.0872 | 12.53 | |
| TEG6 | n-type | 143.74 | 7.7 | 0.1047 | 15.05 | 3853.44 |
| | p-type | 143.74 | 7.7 | 0.1047 | 15.05 | |
| TEG7 | n-type | 132.05 | 6.93 | 0.0942 | 12.45 | 3025.62 |
| | p-type | 119.82 | 6.87 | 0.0934 | 11.2 | |
| TEG8 | n-type | 464.96 | 3.92 | 0.0533 | 24.79 | 6681.54 |
| | p-type | 214.41 | 9.4 | 0.1278 | 27.41 | |

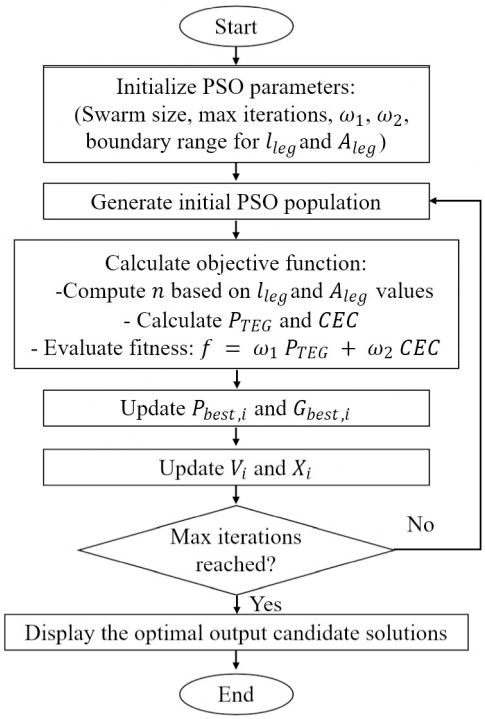


**Figure 2.** The framework of the PSO algorithm considered in the present study.

Figure 3 presents a comprehensive analysis of various TEG materials, highlighting their composition, density, and cumulative CEC. The analysis considers eight different TEG modules, each utilizing distinct n-type and p-type semiconductor materials, including silicon-germanium (Si-Ge), bismuth telluride (Bi-Te), and lead telluride (Pb-Te), among others. The CEC for each TEG leg is determined based on the embodied energy index obtained from the literature (Refs.[20,51]). The results demonstrate the significant influence of

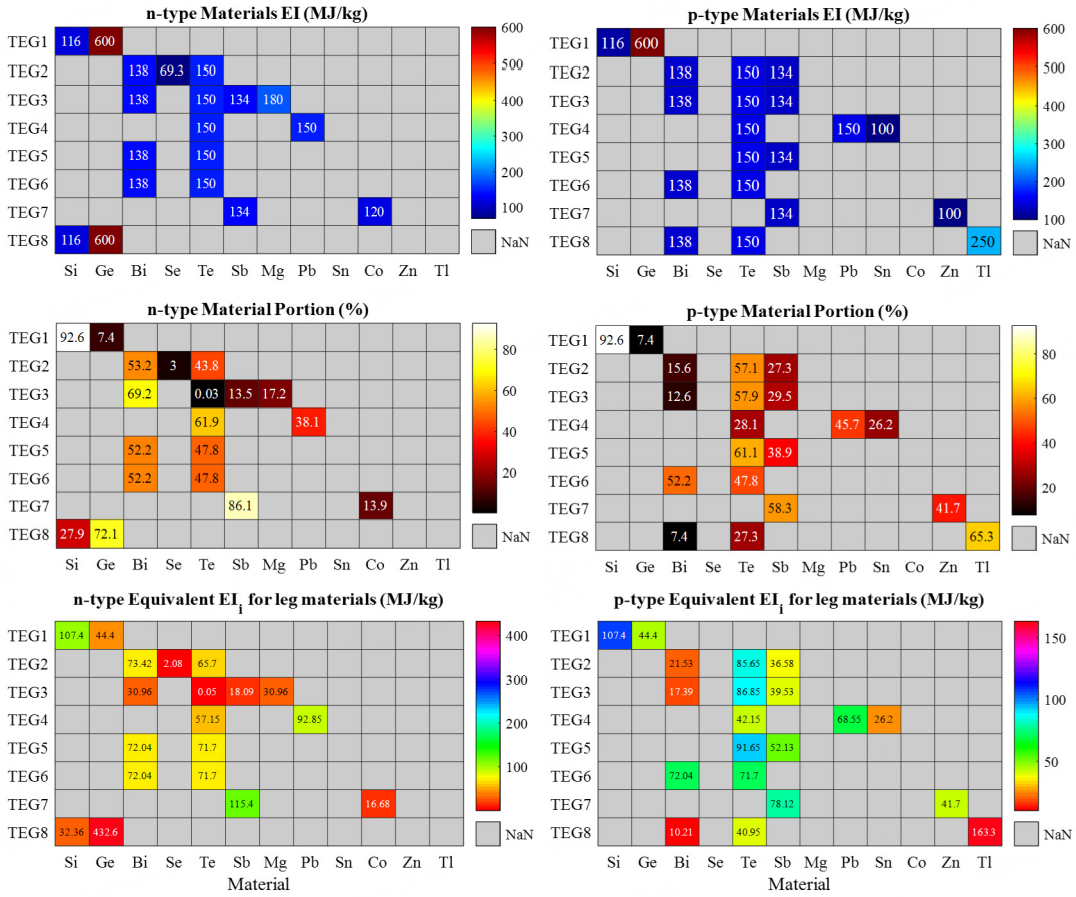


**Figure 3.** Energy inventory of raw materials used in each leg of a TEG.

material portion and composition on the CEC index per TEG leg. Specifically, the embodied energy index of each material within the TEG legs is directly related to its proportion in the leg. Notably, Tl and Ge exhibit the highest embodied energy indices, particularly in TEG8, due to their higher proportions compared to other TEG modules.

On the other hand, the total CEC for each TEG module is presented in Table 3. It is evident that the overall CEC for each leg depends on multiple factors, including composition, density, and the weight of each material. Notably, TEG8 exhibits a significantly high equivalent consumed energy of approximately 24.79 MJ/leg for the n-type leg and 27.41 MJ/leg for the p-type leg. This is primarily attributed to the high embodied energy indices of 464.96 and 214.41 MJ/kg for the n-type and p-type legs, respectively, as well as the increased leg weight. These findings indicate that the manufacturing phase of TEG8 has the highest energy consumption among all TEG systems. Specifically, the energy consumption during the manufacturing phase of TEG8 is approximately 80.78%, 46.61%, 55.24%, 37.34%, 47.19%, 42.33%, and 54.71% higher compared to TEG1 through TEG7, respectively.

Furthermore, the embodied energy of the ceramic layer and copper electrodes was estimated, and the results are summarized in Table 4. The findings indicate that the CEC associated with these components is relatively low, underscoring their minor contribution to the *CEC* of the TEG module. As a result, the overall energy consumption during the manufacturing phase of different TEG modules is predominantly

**Table 4. Equivalent embodied energy for the ceramic cover and the copper electrodes**

| Item | Equivalent $EI_i$ (MJ/kg) | Material volume ($m^3$) | Materials weight (kg) | Quantity | CEC (MJ) |
|---|---|---|---|---|---|
| Ceramic | 18.9[52] | $8 \times 10^{-7}$ | 0.003024 | 2 | 0.1142 |
| Electrode copper | 90[53] | $1.2 \times 10^{-9}$ | $1.0752 \times 10^{-5}$ | 128 | 0.1237 |

influenced by the thermoelectric materials themselves, whereas the impact of ancillary components such as the ceramic and copper layers is negligible. This highlights the critical importance of thermoelectric material selection in determining the embodied energy and overall sustainability of the TEG system.

### Energy output for different TEG modules

The electrical output of different TEG modules depends on several parameters, including the S, n, and ΔT. In this section, the performance of various TEGs is analyzed at ΔT = 30°C, and the obtained results are presented in Figure 4.

Figure 4A presents the electrical output power of different TEG modules. The results indicate that TEG4 exhibits the highest electrical output compared to the other modules, primarily due to its higher Seebeck coefficient. At ΔT = 30 °C, TEG4 generates approximately 0.2134 W, which is 77.413%, 73.383%, 67.291%, 64.058%, 55.248%, 48.782%, and 47.751% higher than TEG1, TEG6, TEG7, TEG2, TEG3, TEG5, and TEG8, respectively. Meanwhile, TEG5 and TEG8 exhibit similar output values of approximately 0.1093 and 0.1115 W, respectively, which can be attributed to their unequal Seebeck coefficients and internal resistances. Meanwhile, TEG5 and TEG8 exhibit similar output values of approximately 0.1093 and 0.1115 W, respectively. This similarity results from a trade-off between their thermoelectric properties, TEG5 has a slightly higher Seebeck coefficient (220 μV/K) but also a higher internal resistance (0.709 Ω), while TEG8 has a slightly lower Seebeck coefficient (217.5 μV/K) but a significantly lower internal resistance (0.442 Ω). The balance between these parameters leads to comparable power output levels. Moreover, although TEG7 produces more power than these three modules, its output is still lower than that of TEG3, TEG4, TEG5, and TEG8. This is attributed to its higher internal resistance, which offsets the benefits of its relatively high Seebeck coefficient. These observations confirm that the power output of a TEG module is influenced by the interplay between its Seebeck coefficient and internal resistance. It is worth pointing out that the power output curve is determined by the interaction between the internal resistance of the TEG module and the external load resistance. According to the maximum power transfer theorem, maximum power output is achieved when the load resistance matches the internal resistance of the module.

The analysis of the electrical output power for various TEG modules highlights the critical influence of both the Seebeck coefficient and internal resistance on overall performance. As illustrated in Figure 4B, the output current decreases linearly with increasing output voltage, reflecting the impact of internal resistance on the slope of the I-V characteristic. Moreover, the output current is not governed by internal resistance alone; it is also influenced by the output voltage, which is itself a function of the Seebeck coefficient and the temperature difference across the module. Therefore, selecting TEG materials with high Seebeck coefficients, in conjunction with optimizing internal resistance, is essential for enhancing performance and maximizing energy conversion efficiency.

### Environmental impact related to the different TEG modules

After evaluating the CEC related to the different TEG materials, investigating its environmental impact is required. In this section, the environmental impact, including the $CO_2$ and GWP is determined and presented in Figure 5A and B, respectively.

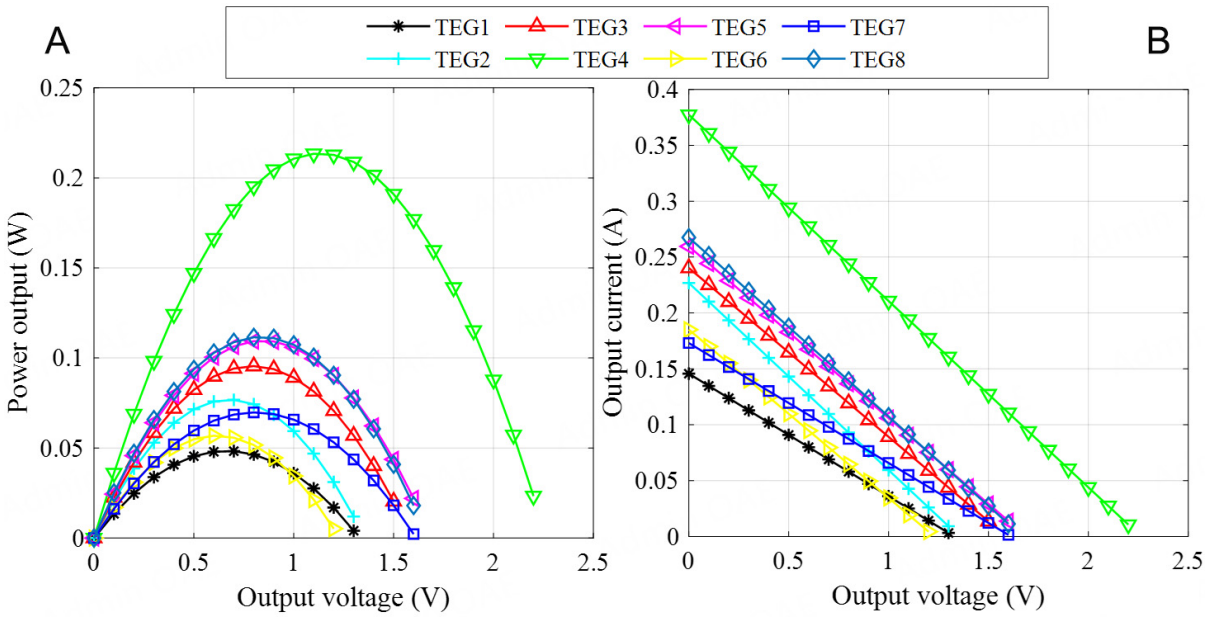


**Figure 4.** Electrical output of the different TEG modules (A) Power-voltage, (B) Current-voltage profiles.

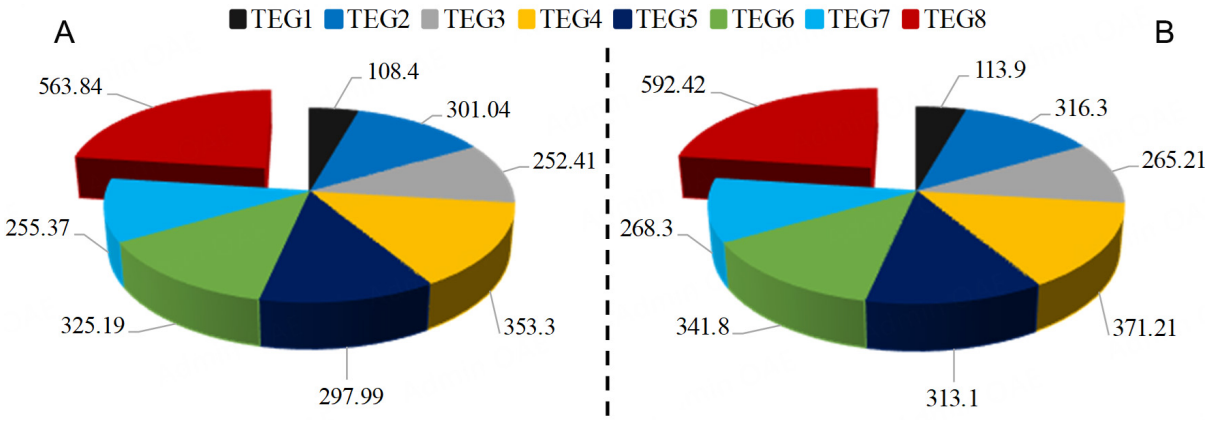


**Figure 5.** Environmental impact related to manufacturing material of TEG module (A) $CO_2$ (kg), (B) GWP (kg.$CO_2$.eq).

Figure 5 illustrates the environmental impact of different TEG module materials, highlighting the significant role of material selection in determining the overall environmental footprint. The results indicate that TEG8 exhibits the highest emissions in terms of both $CO_2$ and GWP, primarily due to its high CEC during the manufacturing phase of its raw materials. In contrast, TEG1 emerges as the most environmentally sustainable option, exhibiting the lowest emissions. Specifically, TEG8 is responsible for 563.84 kg of $CO_2$ emissions and contributes about 592.42 kg.$CO_2$.eq of GWP, which is 420.2% higher than that of TEG1, emphasizes the substantial variation in environmental impact among different TEG materials.

On the other hand, considering that the maximum operating time for the TEG module is 24 h per day and assuming a lifespan of 20 years, as reported in Ref.[54], the equivalent carbon emissions per 1 kWh of energy produced can be analyzed. The results of this analysis are summarized in Table 5.

**Table 5. Equivalent carbon emissions per 1 kWh of energy produced**

| Ref | Energy production (kWh/20 year) | Equivalent kg.$CO_2$/kWh |
|---|---|---|
| TEG1 | 8.45 | 12.8 |
| TEG2 | 13.45 | 22.4 |
| TEG3 | 16.729 | 15.1 |
| TEG4 | 37.39 | 9.5 |
| TEG5 | 19.16 | 15.6 |
| TEG6 | 9.96 | 32.66 |
| TEG7 | 12.23 | 20.89 |
| TEG8 | 19.54 | 28.86 |

Table 5 shows that different TEG modules exhibit varying rates of equivalent $CO_2$ emissions per unit of energy produced (kWh). The results indicate that while TEG8 records the highest total emissions, it ranks second in terms of equivalent carbon emissions per Wh of energy produced. This can be attributed to its higher estimated electrical output over its lifespan. Conversely, TEG6 exhibits the highest equivalent carbon emissions per kWh, primarily due to its lower performance than other TEG modules. On the other hand, TEG4 emerges as the most environmentally sustainable option, as it has the lowest equivalent carbon emissions among all TEG modules. Specifically, producing 1 kWh of electricity using TEG4 results in 9.5 kg of $CO_2$ emissions, which is 3.44 times lower than the equivalent carbon emissions produced by TEG6.

The analysis of equivalent carbon emissions among different TEG modules underscores the significant influence of material selection and energy efficiency on environmental sustainability. The results highlight the importance of optimizing TEG materials and designs to enhance energy efficiency while minimizing environmental impact. Future research should focus on improving TEG performance and exploring eco-friendly materials to reduce their carbon footprint.

### Geometric optimization

After evaluating the overall performance of different TEG modules and their environmental impact associated with manufacturing phases of various materials, the results indicate varying performance for the same system geometry. The TEG geometry considered in the previous section corresponds to a commercially available TEG system. Therefore, optimizing the system geometry is necessary to achieve higher power output while minimizing carbon emissions. This section presents the results obtained for the optimized system geometry.

### Optimized geometry

The present optimization is based on the p- and n-type leg geometry, considering dimensions such as the number of thermocouples, leg length, and cross-sectional area. The obtained results are summarized in Table 6. As observed, the optimization of the TEG geometry results in different values for leg length, cross-sectional area, and the number of thermocouples, all of which significantly influence the power output and environmental impact of the system.

The results indicate that the optimized leg length for the different TEG modules varies between 2 and 4 mm. Specifically, TEG2, TEG3, TEG4, TEG5, and TEG8 feature shorter legs (2 mm) and a higher number of thermocouples (290 or more). In contrast, TEG1, TEG6, and TEG7 have longer legs (4 mm) but a significantly lower number of thermocouples (~145-146). This variation suggests a trade-off between thermocouple density and leg length, directly impacting power generation and efficiency. Additionally, the cross-sectional area of the TEG legs varies slightly, ranging from 2.97 to 3 $mm^2$. Among these

**Table 6. The optimized leg dimension and size of the TEG module**

| Ref | Optimal leg length (mm) | Cross-sectional area ($mm^2$) | Number of thermocouples | TEG module dimension ($cm^2$) |
|---|---|---|---|---|
| TEG1 | 4 | 2.99 | 145 | 8.96 |
| TEG2 | 2 | 2.99 | 291 | 17.98 |
| TEG3 | 2 | 2.98 | 291 | 17.93 |
| TEG4 | 2 | 2.97 | 293 | 17.99 |
| TEG5 | 2 | 2.97 | 293 | 17.99 |
| TEG6 | 3.99 | 3 | 145 | 8.99 |
| TEG7 | 4 | 2.97 | 146 | 8.96 |
| TEG8 | 2 | 3 | 290 | 17.98 |

configurations, TEG6 and TEG8 feature a cross-sectional area of 3 $mm^2$, which provides a lower electrical resistance and improved thermal conduction. Notably, a larger cross-sectional area helps reduce electrical resistance, thereby enhancing electrical performance. However, it also increases thermal conductivity, which reduces the temperature gradient across the TEG sides, potentially affecting overall efficiency.

On the other hand, the size of the TEG module is determined by considering the cross-sectional area, the number of thermocouples, and the spacing between them. As shown in Table 6, the TEG dimensions are primarily influenced by the cross-sectional area and the number of thermocouples. A lower number of thermocouples requires less space, making these modules suitable for applications with spatial constraints. However, TEG modules with larger thermocouples occupy more space but provide enhanced heat-to-electricity conversion, resulting in improved performance.

### Energy assessment and environmental impact

After optimizing the leg dimensions for different TEGs, evaluating the CEC, power production, and environmental impact based on the optimized values is necessary. The obtained results are summarized in Table 7. The results based on the optimized geometry for different TEG modules show an improvement in power production of approximately 22% for TEG1, TEG6, and TEG7. Meanwhile, TEG2, TEG3, TEG4, TEG5, and TEG8 exhibit an improvement of 80% in power production compared to the geometry of the commercial TEG module. The results also indicate a slight reduction in the total energy consumption during the manufacturing phase of the optimized TEG modules compared to the commercial module geometry. This decrease in the CEC of the TEG modules leads to a reduction in $CO_2$ emissions by approximately 0.41, 0.14, 0.91, 0.08, 0.06, 0.96, 0.93, and 0.26 MJ for TEG1, TEG2, TEG3, TEG4, TEG5, TEG6, TEG7, and TEG8, respectively, compared to the emissions during the manufacturing phase of the initial geometry.

To assess the environmental feasibility of various TEG modules, their equivalent $CO_2$ emissions under a temperature difference of $\Delta T = 30$ K are compared with those of other renewable energy systems reported in the literature. Given that TEG modules are solid-state devices with operational characteristics similar to PV systems, the environmental impact of the different TEG modules is specifically compared to that of PV systems to ensure a more practical and meaningful assessment.

As shown in Table 7, the TEG modules exhibit higher equivalent $CO_2$ emissions per kWh compared to several renewable energy systems documented in existing literature. For instance, Ref.[2] reports that a concentrated PV system emits approximately 0.105 kg.$CO_2$/kWh. This represents only 1.12%, 2.58%, 2.58%, 6.2%, 3.77%, 0.44%, 0.69%, and 1.99% of the emissions from TEG1 to TEG8, respectively. These results indicate a relatively lower environmental feasibility for the TEG modules under the given conditions.

**Table 7. Energy assessment and environmental impact for the different TEG modules**

| Ref | Total CEC for TEG module (MJ) | Maximum output (W) | Energy production (kWh/20 year) | $CO_2$ amount (kg) | Equivalent kg.$CO_2$ /kWh |
|---|---|---|---|---|---|
| TEG1 | 1,279.66 | 0.062 | 10.85 | 107.99 | 9.96 |
| TEG2 | 3,566.03 | 0.397 | 69.52 | 300.9 | 4.33 |
| TEG3 | 2,979.93 | 0.494 | 86.47 | 251.5 | 2.91 |
| TEG4 | 4,185.63 | 1.119 | 196.05 | 353.22 | 1.8 |
| TEG5 | 3,530.43 | 0.574 | 100.62 | 297.93 | 2.96 |
| TEG6 | 3,842.06 | 0.073 | 12.78 | 324.23 | 25.37 |
| TEG7 | 3,015.06 | 0.091 | 15.9 | 254.44 | 16 |
| TEG8 | 6,678.43 | 0.573 | 100.45 | 563.58 | 5.61 |

However, increasing the ΔT can enhance the energy output of TEGs and thus reduce their equivalent emissions. Indeed, at ΔT = 100 K, the equivalent $CO_2$ emissions for TEG1 to TEG8 are significantly reduced to approximately 0.114, 0.201, 0.135, 0.085, 0.14, 0.29, 0.187, and 0.26 kg $CO_2$/kWh, respectively. Therefore, the environmental sustainability of different TEG modules is highly dependent on both material selection and operating conditions, particularly the ΔT.

Overall, the design of TEG modules requires careful consideration of leg dimensions and the number of thermocouples. Shorter legs with a high number of thermocouples emerge as the most effective choice for enhancing power output. Conversely, longer legs with low thermocouple numbers may be preferable for reducing the environmental impact associated with the manufacturing phase. Therefore, the optimal trade-off depends on the specific objective, whether prioritizing higher power output or sustainability. In addition, the TEG module dimensions play a critical role in balancing power output, space efficiency, and thermal management. The choice of a specific TEG module should be based on the intended application, available heat source, and installation constraints.

## CONCLUSION

This study presents a comprehensive assessment of TEG materials and system geometries, highlighting the critical trade-offs between performance and environmental sustainability. Through life cycle assessment, we demonstrate that material selection substantially influences embodied energy and GHG emissions, with SiGe-based TEGs exhibiting the highest carbon footprint. PbTe-based TEGs offer the highest energy output, while $Bi_2Te_3$-based modules provide a balance between performance and environmental impact. The PSO-based optimization approach significantly improves power output while reducing environmental impact, underscoring the importance of multi-objective optimization in sustainable TEG development. The findings suggest that optimizing system geometry, particularly through thermocouple count and leg dimensions adjustments, enhances energy conversion and eco-friendliness. These results offer actionable insights for researchers, engineers, and policymakers aiming to develop high-performance, environmentally responsible thermoelectric energy systems.

## DECLARATIONS

### Acknowledgments

The authors gratefully acknowledge the financial assistance provided for the successful completion of this work.

### Authors' contributions

Methodology, investigation, formal analysis, data curation, writing - original draft: Lekbir, A.
Methodology, supervision, writing - review & editing, project administration, funding Acquisition: Mekhilef, S.
Concept, supervision, writing - review & editing: Tey, K. S.; Albaker, A.

### Availability of data and materials

All datasets generated for this study are included in the article.

### Financial support and sponsorship

This research was supported by the Universiti Malaya Matching Grant: MG043-2024.

### Conflicts of interest

All authors declared that there are no conflicts of interest.

### Ethical approval and consent to participate

Not applicable.

### Consent for publication

Not applicable.



## REFERENCES

1. Khenfer, R.; Lekbir, A.; Rouabah, Z.; et al. Experimental investigation of water-based photovoltaic/thermal-thermoelectric hybrid system: energy, exergy, economic and environmental assessment. *J. Power. Sources.* **2024**, *598*, 234151. DOI
2. Lekbir, A.; Hassani, S.; Mekhilef, S. Techno-economic and life cycle assessment of a nanofluid-based concentrated Photovoltaic/Thermal-Thermoelectric hybrid system. *J. Power. Sources.* **2024**, *595*, 234066. DOI
3. Gielen, D.; Boshell, F.; Saygin, D.; Bazilian, M. D.; Wagner, N.; Gorini, R. The role of renewable energy in the global energy transformation. *Energy. Strategy. Rev.* **2019**, *24*, 38-50. DOI
4. Mehta, P.; Gaur, A.; Kumar, C.; Nella, A.; Bhowmick, A.; Rajagopal, M. Energy harvesting techniques and trends in electronic applications. In: Nella A, Bhowmick A, Kumar C, Rajagopal M, editors. Energy harvesting trends for low power compact electronic devices. Cham: Springer International Publishing; 2023. pp. 205-20. DOI
5. Muchuweni, E.; Mombeshora, E. T. Recent advances in thermoelectric performance by incorporating graphene-based materials for energy harvesting. *Renew. Energy. Focus.* **2023**, *45*, 40-52. DOI
6. Xin, J.; Basit, A.; Li, S.; Danto, S.; Tjin, S. C.; Wei, L. Inorganic thermoelectric fibers: a review of materials, fabrication methods, and applications. *Sensors* **2021**, *21*, 3437. DOI PubMed PMC
7. Mamur, H.; Dilmaç, Ö. F.; Begum, J.; Bhuiyan, M. R. A. Thermoelectric generators act as renewable energy sources. *Cleaner. Mater.* **2021**, *2*, 100030. DOI
8. Olabi, A.; Al-Murisi, M.; Maghrabie, H. M.; et al. Potential applications of thermoelectric generators (TEGs) in various waste heat recovery systems. *Int. J. Thermofluids.* **2022**, *16*, 100249. DOI
9. Manghwar, R.; Selvaraj, J.; Abd Rahim, N.; Kumar, L.; Khoharo, H. Global advancements of solar thermoelectric generators application, limitations, and prospects: a comprehensive review. *Appl. Therm. Eng.* **2024**, *257*, 124231. DOI
10. Rjafallah, A.; Younis, A.; Cotfas, D. T.; Cotfas, P. A. Effects of temperature uniformity and nonuniformity on thermoelectric generator performance across hot and cold sides. *Case. Stud. Therm. Eng.* **2024**, *59*, 104596. DOI
11. Lekbir, A.; Hassani, S.; Ab Ghani, M. R.; Gan, C. K.; Mekhilef, S.; Saidur, R. Improved energy conversion performance of a novel design of concentrated photovoltaic system combined with thermoelectric generator with advance cooling system. *Energy. Convers. Manag.* **2018**, *177*, 19-29. DOI
12. Shi, X.; Cao, T.; Chen, W.; et al. Advances in flexible inorganic thermoelectrics. *EcoEnergy* **2023**, *1*, 296-343. DOI
13. Zheng, Z.; Shi, X.; Ao, D.; et al. Harvesting waste heat with flexible $Bi_2Te_3$ thermoelectric thin film. *Nat. Sustain.* **2023**, *6*, 180-91. DOI
14. Chen, Y. X.; Shi, X. L.; Zhang, J. Z.; et al. Deviceization of high-performance and flexible $Ag_2Se$ films for electronic skin and servo rotation angle control. *Nat. Commun.* **2024**, *15*, 8356. DOI PubMed PMC

15. Zhang, M.; Shi, X.; Liu, S.; et al. Compositing effect leads to extraordinary performance in GeSe-based thermoelectrics. *Adv. Funct. Mater.* **2025**, 2500898. DOI
16. Hu, B.; Shi, X. L.; Cao, T.; et al. Realizing high performance in flexible $Mg_3Sb_{2-x}Bi_x$ thin-film thermoelectrics. *Adv. Sci.* **2025**, e2502683. DOI
17. Chan, Z.; Lim, J. H. Life cycle analysis of thermoelectric generator efficiency for waste heat recovery. *AIP. Conf. Proc.* **2020**, *2233*, 020003. DOI
18. Lan, Y.; Lu, J.; Wang, S. Study of the geometry and structure of a thermoelectric leg with variable material properties and side heat dissipation based on thermodynamic, economic, and environmental analysis. *Energy* **2023**, *282*, 128895. DOI
19. Ibn-Mohammed, T.; Koh, S.; Mustapha, K.; et al. Techno-environmental analysis of material substitution in thermoelectric modules: non-oxide (bismuth telluride alloys) vs. oxide-based (lanthanum-doped strontium titanate and calcium cobaltite) materials. *Energy. Convers. Manag. X.* **2023**, *19*, 100395. DOI
20. Soleimani, Z.; Zoras, S.; Ceranic, B.; Shahzad, S.; Cui, Y. The cradle to gate life-cycle assessment of thermoelectric materials: A comparison of inorganic, organic and hybrid types. *Sustain. Energy. Technol. Assess.* **2021**, *44*, 101073. DOI
21. Dhawan, R.; Madusanka, P.; Hu, G.; et al. $Si_{0.97}Ge_{0.03}$ microelectronic thermoelectric generators with high power and voltage densities. *Nat. Commun.* **2020**, *11*, 4362. DOI PubMed PMC
22. Pavlovskaya, N. T.; Litovchenko, P. G.; Ugrin, Y. O.; Pavlovskyy, Y. V.; Ostrovskii, I. P.; Rogacki, K. Magnetoresistance of proton irradiated $Si_{0.97}Ge_{0.03}$ whiskers. *Mod. Electron. Mater.* **2016**, *2*, 85-8. DOI
23. Parashchuk, T.; Kostyuk, O.; Nykyruy, L.; Dashevsky, Z. High thermoelectric performance of p-type $Bi_{0.5}Sb_{1.5}Te_3$ films on flexible substrate. *Mater. Chem. Phys.* **2020**, *253*, 123427. DOI
24. Lemine, A. S.; El-Makaty, F. M.; Al-Ghanim, H. A.; Youssef, K. M. Experimental and modeling analysis of p-type $Bi_{0.4}Sb_{1.6}Te_3$ and graphene nanocomposites. *J. Mater. Res. Technol.* **2022**, *16*, 1702-12. DOI
25. Amin, A.; Huang, R.; Newbrook, D.; et al. Screen-printed bismuth telluride nanostructured composites for flexible thermoelectric applications. *J. Phys. Energy.* **2022**, *4*, 024003. DOI
26. Liang, J.; Shi, X.; Peng, Y.; et al. Synergistic effect of band and nanostructure engineering on the boosted thermoelectric performance of n-type $Mg_{3+\delta}(Sb, Bi)_2$ Zintls. *Adv. Energy. Mater.* **2022**, *12*, 2201086. DOI
27. Imasato, K.; Fu, C.; Pan, Y.; et al. Metallic n-type $Mg_3Sb_2$ single crystals demonstrate the absence of ionized impurity scattering and enhanced thermoelectric performance. *Adv. Mater.* **2020**, *32*, e1908218. DOI
28. Varghese, T.; Dun, C.; Kempf, N.; et al. Flexible thermoelectric devices of ultrahigh power factor by scalable printing and interface engineering. *Adv. Funct. Mater.* **2020**, *30*, 1905796. DOI
29. Pandit, A.; Haleoot, R.; Hamad, B. Structural, electronic and thermoelectric properties of $Pb_{1-x}Sn_xTe$ alloys. *J. Electron. Mater.* **2020**, *49*, 586-92. DOI
30. Kungumadevi, L.; Sathyamoorthy, R. Structural, electrical, and optical properties of PbTe thin films prepared by simple flash evaporation method. *Adv. Condens. Matter. Phys.* **2012**, *2012*, 1-5. DOI
31. Norimasa, O.; Chiba, T.; Hase, M.; Komori, T.; Takashiri, M. Improvement of thermoelectric properties of flexible $Bi_2Te_3$ thin films in bent states during sputtering deposition and post-thermal annealing. *J. Alloys. Compd.* **2022**, *898*, 162889. DOI
32. Park, D.; Park, S.; Jeong, K.; Jeong, H. S.; Song, J. Y.; Cho, M. H. Thermal and electrical conduction of single-crystal $Bi_2Te_3$ nanostructures grown using a one step process. *Sci. Rep.* **2016**, *6*, 19132. DOI PubMed PMC
33. Sun, Z.; Cheng, K.; Lin, S.; et al. Stoichiometric effect of $Sb_2Te_3$ thin film on thermoelectric property. *ACS. Appl. Energy. Mater.* **2022**, *5*, 7026-33. DOI
34. Endo, R.; Maeda, S.; Jinnai, Y.; et al. Electric resistivity measurements of $Sb_2Te_3$ and $Ge_2Sb_2Te_5$ melts using four-terminal method. *Jpn. J. Appl. Phys.* **2010**, *49*, 065802. DOI
35. Liu, Z.; Zhu, J.; Tong, X.; Niu, S.; Zhao, W. A review of $CoSb_3$-based skutterudite thermoelectric materials. *J. Adv. Ceram.* **2020**, *9*, 647-73. DOI
36. Bourgès, C.; Zhang, W.; Raut, K. K.; et al. Investigation of Mn single and Co-doping in thermoelectric $CoSb_3$-skutterudite: a way toward a beneficial composite effect. *ACS. Appl. Energy. Mater.* **2023**, *6*, 9646-56. DOI
37. Lin, J.; Ma, L.; Liu, Q.; et al. Continuous phase transition in thermoelectric $Zn_4Sb_3$. *Mater. Today. Energy.* **2021**, *21*, 100787. DOI
38. Zou, T.; Qin, X.; Zhang, Y.; et al. Enhanced thermoelectric performance of β-$Zn_4Sb_3$ based nanocomposites through combined effects of density of states resonance and carrier energy filtering. *Sci. Rep.* **2015**, *5*, 17803. DOI PubMed PMC
39. Fatima, K.; Noor, H.; Ali, A.; Monakhov, E.; Asghar, M. Annealing effect on seebeck coefficient of SiGe thin films deposited on quartz substrate. *Coatings* **2021**, *11*, 1435. DOI
40. Fan, Z.; Liang, J.; Chen, J.; et al. Realizing high thermoelectric performance for p-type SiGe in medium temperature region via TaC compositing. *J. Materiomics.* **2023**, *9*, 984-91. DOI
41. Yamanaka, S.; Kosuga, A.; Kurosaki, K. Thermoelectric properties of $Tl_9BiTe_6$. *J. Alloys. Compd.* **2003**, *352*, 275-8. DOI
42. Lekbir, A.; Meddad, M. A. E.; Benhadouga, S.; Khenfer, R. Higher-efficiency for combined photovoltaic-thermoelectric solar power generation. *Int. J. Green. Energy.* **2019**, *16*, 371-7. DOI
43. Vovchenko, L.; Matzui, L.; Zhuravkov, A.; Samchuk, A. Electrical resistivity of compacted TEG and TEG-Fe under compression. *J. Phys. Chem. Solids.* **2006**, *67*, 1168-72. DOI
44. Hammond, G. P.; Jones, C. I. Embodied energy and carbon in construction materials. *Proc. Inst. Civ. Eng. Energy.* **2008**, *161*, 87-98. DOI

45. William, D. C. J.; David, G. R. Materials science and engineering: an introduction, 10th edition; 2018. Available from: https://www.wiley.com/en-us/Materials+Science+and+Engineering%3A+An+Introduction%2C+10th+Edition-p-9781119405498 [Last accessed on 12 May 2025].
46. Ashby, M. F. Materials and the environment: eco-informed material choice. Elsevier; 2012. Available from: https://www.sciencedirect.com/book/9780123859716/materials-and-the-environment [Last accessed on 14 May 2025]
47. Schivley, G.; Ingwersen, W. W.; Marriott, J.; Hawkins, T. R.; Skone, T. J. Identifying/quantifying environmental trade-offs inherent in GHG reduction strategies for coal-fired power. *Environ. Sci. Technol.* **2015**, *49*, 7562-70. DOI PubMed
48. Jeong, B.; Jeon, H.; Kim, S.; Kim, J.; Zhou, P. Evaluation of the lifecycle environmental benefits of full battery powered ships: comparative analysis of marine diesel and electricity. *J. Mar. Sci. Eng.* **2020**, *8*, 580. DOI
49. Wang, X.; Ting, D. S.; Henshaw, P. Mutation particle swarm optimization (M-PSO) of a thermoelectric generator in a multi-variable space. *Energy. Convers. Manag.* **2020**, *224*, 113387. DOI
50. Xu, G.; Cui, Q.; Shi, X.; et al. Particle swarm optimization based on dimensional learning strategy. *Swarm. Evol. Comput.* **2019**, *45*, 33-51. DOI
51. Ashby, M.; Melia, H.; Figuerola, M.; Gorsse, S.; Philips, L. The CES EduPack materials science and engineering package. 2018. Available from: https://www.researchgate.net/profile/Hannah-Melia/publication/331983339_The_CES_EduPack_Materials_Science_and_Engineering_Package/links/5c98f51f45851506d72bab88/The-CES-EduPack-Materials-Science-and-Engineering-Package.pdf [Last accessed on 14 May 2025].
52. Embodied energy. Available from: https://www.yourhome.gov.au/materials/embodied-energy [Last accessed on 12 May 2025].
53. UNEP. Environmental risks and challenges of anthropogenic metals flows and cycles; 2013. Available from: https://www.yourhome.gov.au/materials/embodied-energy [Last accessed on 14 May 2025]
54. Jaziri, N.; Boughamoura, A.; Müller, J.; Mezghani, B.; Tounsi, F.; Ismail, M. A comprehensive review of thermoelectric generators: technologies and common applications. *Energy. Rep.* **2020**, *6*, 264-87. DOI